Confocal imaging of transmembrane voltage by SEER of di-8-ANEPPS

Carlo Manno,[1] Lourdes Figueroa,[1] Robert Fitts,[2] and Eduardo Ríos[1]

[1]Section of Cellular Signaling, Department of Molecular Biophysics and Physiology, Rush University, Chicago, IL 60612
[2]Department of Biology, Marquette University, Milwaukee, WI 53233

Imaging, optical mapping, and optical multisite recording of transmembrane potential (V_m) are essential for studying excitable cells and systems. The naphthylstyryl voltage-sensitive dyes, including di-8-ANEPPS, shift both their fluorescence excitation and emission spectra upon changes in V_m. Accordingly, they have been used for monitoring V_m in nonratioing and both emission and excitation ratioing modes. Their changes in fluorescence are usually much less than 10% per 100 mV. Conventional ratioing increases sensitivity to between 3 and 15% per 100 mV. Low sensitivity limits the value of these dyes, especially when imaged with low light systems like confocal scanners. Here we demonstrate the improvement afforded by shifted excitation and emission ratioing (SEER) as applied to imaging membrane potential in flexor digitorum brevis muscle fibers of adult mice. SEER—the ratioing of two images of fluorescence, obtained with different excitation wavelengths in different emission bands—was implemented in two commercial confocal systems. A conventional pinhole scanner, affording optimal setting of emission bands but less than ideal excitation wavelengths, achieved a sensitivity of up to 27% per 100 mV, nearly doubling the value found by conventional ratioing of the same data. A better pair of excitation lights should increase the sensitivity further, to 35% per 100 mV. The maximum acquisition rate with this system was 1 kHz. A fast "slit scanner" increased the effective rate to 8 kHz, but sensitivity was lower. In its high-sensitivity implementation, the technique demonstrated progressive deterioration of action potentials upon fatiguing tetani induced by stimulation patterns at >40 Hz, thereby identifying action potential decay as a contributor to fatigue onset. Using the fast implementation, we could image for the first time an action potential simultaneously at multiple locations along the t-tubule system. These images resolved the radially varying lag associated with propagation at a finite velocity.

INTRODUCTION

Imaging of transmembrane potential, V_m, and related techniques of optical mapping and optical multisite recording with voltage-sensitive dyes (Cohen and Salzberg, 1978) are essential tools in the study of excitable cells and systems. They are especially valuable in the study of the spread of excitation in complex multicellular systems, including heart muscle (Rohr and Salzberg 1994; for review see Jalife, 2000) and neural tissue (Zecevic et al., 2003; for review see Peterka et al., 2011), or distributed excitable membranes in a single cell (like the transverse tubule system of striated muscle; Heiny et al., 1983).

Among the dyes most used are the ones in the naphthylstyryl class, including pyridinium, 4-(2-(6-(dibutylamino)-2-naphthalenyl)ethenyl)-1-(3-sulfopropyl)-, hydroxide, inner salt (di-4-ANEPPS) and pyridinium, 4-(2-(6-(dioctylamino)-2-naphthalenyl)ethenyl)-1-(3-sulfopropyl)-, inner salt (di-8-ANEPPS), which respond to changes in potential by electrochromism (Loew and Simpson, 1981). The spectra of electrochromic dyes are altered via a direct coupling of the molecular electronic states with the electric field. In the absence of molecular reorientations the response is rapid. The interaction results in similar shifts for excitation and emission spectra (Fluhler et al., 1985; Fromherz and Lambacher, 1991). These dyes are therefore used ratiometrically, with either excitation or emission switching, to derive a signal that is insensitive to photobleaching and variations of concentration and volume (Bedlack et al., 1992). Because the spectral shifts are small (<5 nm for 100 mV; Kao et al., 2001) and other changes are minor, the signals are typically of small amplitude (Gupta et al., 1981), which limits sensitivity.

Di-8-ANEPPS (Bedlack et al., 1992; structure in Fig. 1 A) was given a large dioctylamino tail to reduce dye internalization, which occurs upon long-term exposure and further complicates and undercuts the sensitivity of the method. Di-8-ANEPPS has been used to measure transmembrane potentials statically and dynamically in cells of many types, including neural (e.g., Zhang et al., 1998), endothelial (Beach et al., 1996), cardiac (Valverde et al., 2010; Tian et al., 2011), and skeletal muscle (Kim and Vergara, 1998; DiFranco et al., 2005, 2011). In these

Correspondence to Eduardo Ríos: erios@rush.edu

Abbreviations used in this paper: AOBS, acousto-optical beam splitter; di-4-ANEPPS, pyridinium, 4-(2-(6-(dibutylamino)-2-naphthalenyl)ethenyl)-1-(3-sulfopropyl)-, hydroxide, inner salt; di-8-ANEPPS, pyridinium, 4-(2-(6-(dioctylamino)-2-naphthalenyl)ethenyl)-1-(3-sulfopropyl)-, inner salt; FDB, flexor digitorum brevis; SEER, shifted excitation and emission ratioing; VSD, voltage-sensitive detector.

The Rockefeller University Press $30.00
J. Gen. Physiol. Vol. 141 No. 3 371–387
www.jgp.org/cgi/doi/10.1085/jgp.201210936

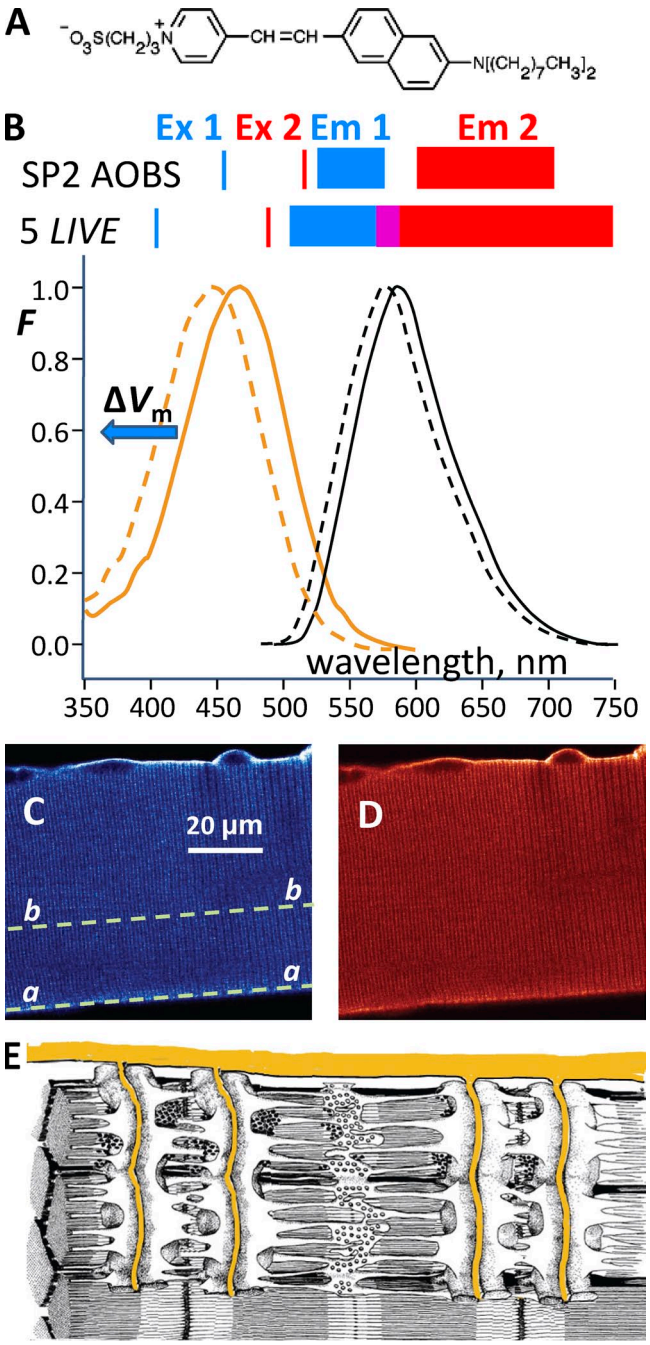

Figure 1. SEER of di-8-ANEPPS fluorescence. (A) Structure of di-8-ANEPPS. (B) Its excitation (orange) and emission spectra. Solid black line, emission spectrum measured in mouse muscle (DiFranco et al., 2005). Solid orange line, excitation spectrum, provided by the manufacturer. Broken lines, estimates by J. Vergara and M. DiFranco (personal communication) of excitation and emission spectra, as shifted upon a depolarization of 100 mV. The diagrams at the top indicate excitation and emission lights in two implementations: in a SP2 AOBS conventional pinhole scanner and in the 5 LIVE slit scanner. Lines labeled Ex1 and Ex2 mark the wavelengths used for excitation: 458 and 514 nm in the SP2, and 405 and 488 nm in the 5 LIVE. Rectangles labeled Em1 and Em2 mark the two wavelength ranges where emitted light was collected (524–580 nm and 602–707 nm for the SP2; 505–565 nm and 580–750 nm for the 5 LIVE). Although the use of diffraction gratings and spectral slits in the SP2 assures sharply defined ranges, the definition in the 5 LIVE, which relies on a limited set of fixed optical elements, is less precise (the purple area in the diagram marks a band of residual overlap). Excitation wavelengths and emission ranges were combined as described in the text to obtain F_{11}, F_{12}, F_{21}, and F_{22}. (C and D) Images of fluorescence $F_{11}(x,y)$ and $F_{22}(x,y)$ in an FDB muscle fiber stained with di-8-ANEPPS, obtained using a small pinhole (1.5 Airy diameters). Dynamic studies required line scan images, which were obtained by scanning along the cell surface, as in line *a-a* of C, using a larger pinhole. ID: 030612a_004. (E) Diagrammatic representation of the membrane systems. Di-8-ANEPPS, present in the extracellular space (orange), will initially stain the plasmalemma and its invaginations, the transverse tubular system. Eventually it will be internalized and also stain the sarcoplasmic reticulum, plus other organelles not shown. Modified from Peachey (1965), with generous help from C.F. Armstrong (University of Pennsylvania, Philadelphia, PA).

studies, the signals of di-8-ANEPPS are derived either from a single emission band (e.g., DiFranco et al., 2011) or ratiometrically (e.g., Knisley et al., 2000). The sensitivity, defined as steady change in relative fluorescence or fluorescence ratio per unit depolarizing change in membrane voltage, is reported at between 0.015 $(100\ mV)^{-1}$ (in the ratiometric measurements of Bullen and Saggau, 1999) and 0.15 $(100\ mV)^{-1}$ (Zhang et al., 1998; Erlichman et al., 2009), or 15% of resting fluorescence ratio per 100 mV.

This sensitivity is sufficient for studies in which light is photometrically collected from large areas, but is limiting when both temporal and spatial details are sought, as in dynamic microscopic imaging. Here we report an alternative method for evoking and collecting signals of di-8-ANEPPS. Shifted excitation and emission ratioing of fluorescence (SEER; Launikonis et al., 2005) enhances dynamic range (*DR*) and sensitivity when a fluorescent sensor shifts both its excitation and emission spectra. The use of SEER results in an ~100% increase in sensitivity in confocal imaging of potential difference across membranes of mouse muscle cells.

We demonstrate the technique using two confocal scanning devices with different virtues and limitations. With one of them, the SP2 acousto-optical beam splitter (AOBS) scanner from Leica, the approach optimizes sensitivity; with the other, the "superfast" slit scanner 5 LIVE, from Carl Zeiss, the approach optimizes temporal resolution. We then demonstrate two applications that take advantage of the respective strengths of these different scanning devices.

MATERIALS, METHODS, AND RESULTS

The fundamentals at work in both implementations of the technique are illustrated with Fig. 1 B. Shown are spectra of di-8-ANEPPS (provided by M. DiFranco and J. Vergara, University of California, Los Angeles, Los Angeles, CA) in cells at rest and after depolarization.

When, as in this case, both spectra of an indicator shift, SEER provides a better signal than either the emission or excitation ratio. (These spectra were put together from different sources, as described in the figure legend, and are only approximate. They provide, however, important clues for the initial design of the method, which was later optimized empirically.)

At the top of Fig. 1 B, we represented the excitation and emission lights in our two implementations: first in a conventional pinhole confocal laser scanner (SP2 AOBS; Leica) and then in the 5 LIVE, a so-called "superfast" slit scanner (Carl Zeiss). Both systems control laser intensity with acousto-optical filters, which allows for alternation of exciting light between lines of an x-y scan or a line scan, yielding images with alternate excitation that are essentially simultaneous. Ex1 and Ex2 are the two laser lines used, which are different in the two systems; Em1 and Em2 are the corresponding emission bands, which are also different. By combining these excitation wavelengths and emission bands, four light signals are obtained—F_{11}, F_{12}, F_{21}, and F_{22}—where the first subindex designates the excitation line and the second designates the emission band. Although the SP2 scanner has AOBSs and spectral decomposition of the emitted light, which permitted a protocol closer to the ideal, the slit scanner has only fixed optical components, which resulted in a less efficient protocol (hampered by imperfect separation of emission bands). The implementation on the slit scanner proved valuable instead for its extraordinary temporal resolution.

SEER of di-8-ANEPPS in a conventional pinhole scanner

To implement the technique, cells enzymatically isolated from mouse flexor digitorum brevis (FDB) muscle are stained by brief exposure to a saline with di-8-ANEPPS and then washed in Tyrode's solution. Fig. 1 E shows diagrammatically the membranes, plasmalemma and t-tubules, that the dye will initially stain. Fig. 1 (C and D) shows x-y scans of F_{11} and F_{22}, featuring the high spatial resolution achieved with a small pinhole. The dynamic experiments instead require line scanning at maximal speed, which limits light intensity. In these, a large pinhole was used. Line scanning could be done along the fiber surface (Fig. 1 C, line *a-a*), but in most cases was done deep inside the cell, along lines (*b-b*) as parallel as possible to the fiber axis, monitoring the fluorescence of dye that was largely staining transverse tubules.

The advantages of SEER over conventional ratioing are demonstrated in Fig. 2. The stained muscle fiber was field stimulated (for 350 ms at 40 Hz) to produce a train of action potentials. The confocal scanner acquired line scan images of fluorescence in the ranges Em1 and Em2 simultaneously. Scanning of fluorescence was bidirectional, at 500 µs per line, with the excitation light alternating between Ex1 in left-to-right scanning and Ex2 in the return trip ("line interleaving"). Four line scan images, $F_{11}(x,t)$, $F_{12}(x,t)$, $F_{21}(x,t)$, and $F_{22}(x,t)$, were thereby acquired nearly simultaneously.

Fig. 2 A shows a subset of the $F_{22}(x,t)$ image (normalized to eliminate inhomogeneities of staining, as described in the figure legend). Its line average, $F_{22}(t)$, is plotted in Fig. 2 B with the red trace, together with a similarly obtained $F_{11}(t)$, in blue. Fig. 2 (C and D) shows $F_{22}(t)/F_{21}(t)$, one of two possible emission ratios, and $F_{22}(t)/F_{12}(t)$, an excitation ratio. Finally in Fig. 2 E is $F_{22}(t)/F_{11}(t)$, the SEER ratio. F_{22}/F_{11} decreases by up to 33% at the peak of the action potentials. By comparison, the emission and excitation ratios change by no more than 22%. Theory, developed next, clarifies the reasons for the enhanced sensitivity of SEER and predicts the magnitude of the improvement.

Theory

The logarithmic (or normalized) sensitivity of a ratiometric monitor of concentration can be defined as

$$S_L \equiv \frac{1}{R}\frac{dR}{dC},$$

where C represents the monitored variable and R represents the monitor signal (ratio).

To extend this definition to voltage-sensitive detectors (VSDs), consider first a definition of sensitivity applied usually to sensors, whether ratiometric or not:

$$S_L \equiv \frac{1}{F}\frac{dF}{dV} \approx \frac{1}{F_0}\frac{\Delta F}{\Delta V}.$$

Sensitivity defined this way may be positive or negative and is usually measured in the units $(100\ \text{mV})^{-1}$, a.k.a., "percent per mV." Electrochromic VSDs, a group that includes di-8-ANEPPS, have typical values of 0.05–0.15 $(100\ \text{mV})^{-1}$, although examples with greater sensitivity will be considered later. Sensitivity varies slowly with voltage between −100 and 100 mV (e.g., Fromherz et al., 2008) and increases in absolute value at the red tail of the excitation spectrum (Kuhn et al., 2004).

A first improvement in sensitivity, feasible with sensors that shift their spectra, is ratioing of signals in two wavelength ranges. In the case of electrochromic dyes, it is usually possible to find two regions (for excitation or emission) where depolarization has opposite effects on F. We will designate these regions with subindexes 2 (for the region where depolarization causes a decrease in F) and 1 (where the opposite occurs). Thus, defining the sensitivities in these two regions as S_{L2} and S_{L1}, it is possible to analogously define the sensitivity of the ratio F_2/F_1, and force it to be positive, as follows:

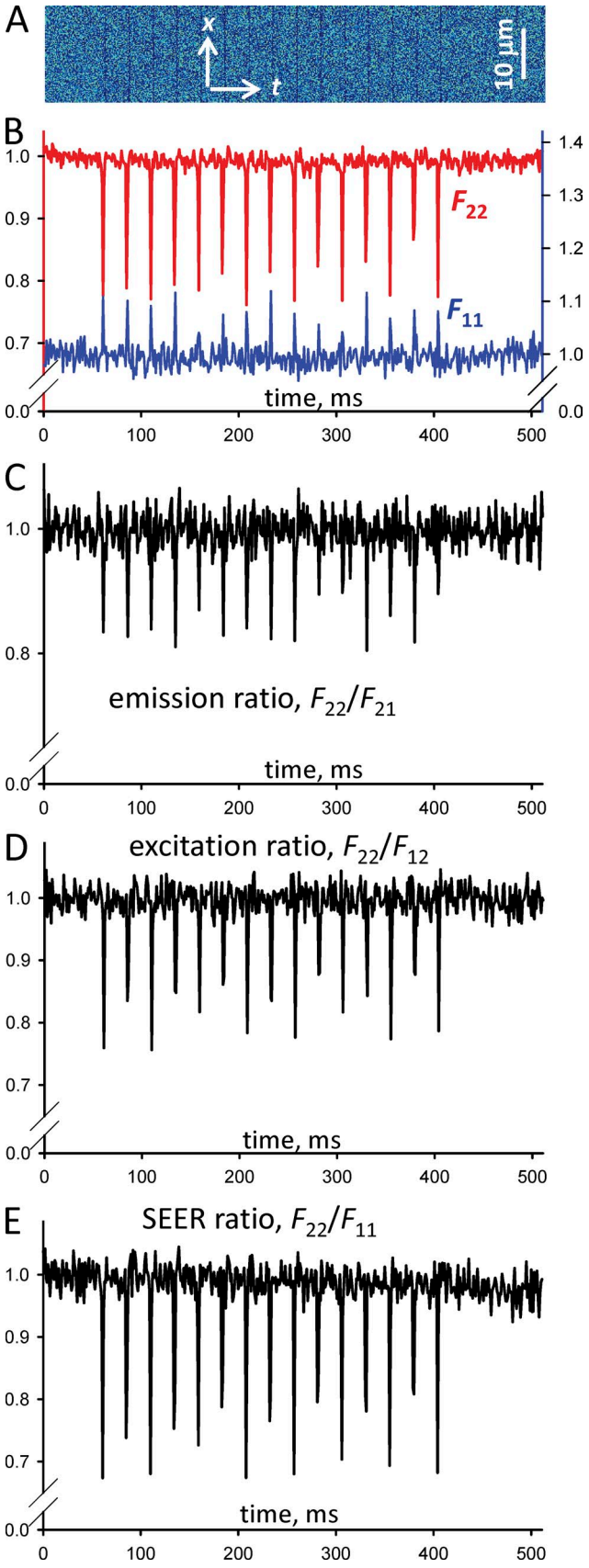

Figure 2. Alternative ratiometric signals. (A) Line scan image of fluorescence $F_{22}(x,t)$, corrected for bleaching and staining inhomogeneity, then cropped and resized for convenience of presentation, acquired in emission range Em2 upon excitation with Ex1 (Fig. 1 B). While the images were being acquired, a train of 15 field stimuli was applied at a frequency of 40 Hz. (B) The spatial average $F_{22}(t)$ of $F_{22}(x,t)$. (C) The spatially averaged emission ratio, of $F_{22}(t)$ by the corresponding average of $F_{21}(x,t)$, acquired simultaneously in emission range Em1. (D) The averaged excitation ratio, of $F_{22}(t)$ by the average of $F_{12}(x,t)$, acquired in the same emission range while excited by Ex1. (E) The SEER ratio, $F_{22}(t)/F_{11}(t)$, which produces the greatest signals among all possible combinations. The ordinate scales of graphs B–D are chosen to make the span of the transients approximately proportional to the relative change in ratio. ID: 030612a_049.

$$S_L \equiv \left|\frac{1}{R}\frac{dR}{dV}\right| = \left|\frac{F_1}{F_2}\frac{d(F_2/F_1)}{dV}\right| = \frac{F_1}{F_2}\frac{F_1|dF_2| + F_2 dF_1}{F_1^2}\frac{1}{dV} = |S_{L2}| + S_{L1}. \quad (1)$$

Therefore, ratiometry combines by addition the sensitivities in the two spectral regions that provide the ratioed signals. This is but one of its virtues; ratiometry also rejects interferences and noise that are common to both channels (but note the qualification of this virtue in the section describing the implementation of the technique at high temporal resolution).

An additional improvement in sensitivity is achieved by the SEER method. The expression that follows, where the two subindexes represent excitation and emission, respectively, is the definition of SEER:

$$R \equiv \frac{F_{22}}{F_{11}} = \frac{F_{22}}{F_{21}} \times \frac{F_{21}}{F_{11}} = R_{em} \times R_{ex}. \quad (2)$$

Eq. 2 can be substituted in Eq. 1 to obtain

$$S_L \equiv \left|\frac{1}{R_{em}R_{ex}}\frac{d(R_{em}R_{ex})}{dV}\right| = \left|\frac{1}{R_{em}}\frac{dR_{em}}{dV} + \frac{1}{R_{ex}}\frac{dR_{ex}}{dV}\right|, \quad (3)$$

which simplifies to

$$S_L \equiv S_{L,\,em} + S_{L,\,ex}, \quad (4)$$

provided that both emission and excitation ratios change in the same direction.

Finite differences can be used instead of differentials for a practical definition of sensitivity, namely,

$$S_L \equiv \frac{1}{R_0}\left|\frac{\Delta R}{\Delta V}\right| = \frac{1}{R_{0,em}R_{0,ex}}\left|\frac{\Delta(R_{em}R_{ex})}{\Delta V}\right| = \frac{\left|\Delta\left(R_{em}/R_{0,em}\;\;R_{ex}/R_{0,ex}\right)\right|}{|\Delta V|}. \quad (5)$$

Because Eq. 3 is the local limiting form of Eq. 5, the application of Eq. 5 should yield adequate results when ΔR is small. Here we demonstrate its application, using the example of Fig. 2.

The amplitude of the SEER signal at the peak of the action potential ($|\Delta R|/R_0$, which by Eq. 5 is $S_L \times |\Delta V|$), is 0.33 for the biggest peaks. Considering that the corresponding emission and excitation ratios $R_{em}/R_{0,em}$ and $R_{ex}/R_{0,ex}$ are both close to 0.82 at the peaks, the value of $S_L \times |\Delta V|$ is calculated, by the last term in Eq. 5, as $1 - 0.82^2 = 0.33$. The individually calculated sensitivities $S_{L,em} \times |\Delta V|$ and $S_{L,ex} \times \Delta V$, are $1 - 0.82 = 0.18$. Therefore, the sensitivity of SEER is also approximately equal to the sum of the emission and excitation sensitivities when defined with Eq. 5. In the special case of electrochromic VSDs, for which the emission and excitation sensitivities are similar, SEER improvement is approximately twofold.

Normalization and nomenclature. A convenient consequence of defining sensitivity as a logarithmic derivative is that the absolute value of the ratio (in conventional or SEER modes) becomes largely irrelevant, as S_L and voltage only depend on its relative changes. A practical outcome is that a similar value of S_L is found whether or not the individual fluorescence images used in a ratio are normalized to their initial values (as any linear factor affecting fluorescence cancels in the definition of Eq. 1). Thus, a ratio of normalized fluorescence images,

$$R \equiv \frac{F_{hi}(x,t) / F_{hi}(x,0)}{F_{jk}(x,t) / F_{jk}(x,0)}, \quad (6)$$

where h, i, j, and k are arbitrary subindexes, will be trivially equal to $F_{hi}(x,t)/F_{jk}(x,t)$, and the sensitivity, $|1/R\, dR/dV|$, will have the same value whether or not one or both images used in the calculation are normalized to their initial or baseline value. For the same reason it is possible (and sometimes convenient for maximizing information) to change independently the intensity of either excitation light, which of course changes the measured ratio, without major changes in sensitivity.

The fluorescence images are routinely normalized to the baseline fluorescence, which is the average of $F(x,t)$ over $t < t_0$, the beginning of the first pulse or action potential. Thus, while formally the ratio images were calculated using Eq. 6, they will be simply represented as $R(x,t) = F_{hi}(x,t)/F_{jk}(x,t)$, and their line averages as $R(t) = F_{hi}(t)/F_{jk}(t)$, omitting the arguments when the meaning is clear. It is also convenient to represent R normalized by its baseline average value, R_0, as according to Eq. 1 the change in R/R_0 for a 100-mV pulse is equal to S_L in units of $(100\ mV)^{-1}$.

Calibration

Although the records in Fig. 2 show clearly the increase in sensitivity afforded by SEER ratioing, they also show what appears to be a high variance in the fluorescence signals F_{11} and F_{22}, especially between peaks of the transients associated with successive action potentials. Consequently, the variation in the peaks of the SEER ratio, F_{22}/F_{11}, is also large, and relatively larger than in the nonratioed F_{22}. On first inspection, it seems that the increase in sensitivity achieved by ratioing is rendered useless by a parallel decrease in signal-to-noise ratio.

Closer examination of the records suggests that a large part of the variation between peaks of the ratio signal (Fig. 2 E) is periodic, hence not caused by noise. This variation could be due to inadequate frequency of scanning, which at 1 kHz (as two lines must be acquired to construct one line ratio) cannot effectively sample the high-frequency components of action potentials, resulting in a beat or alias frequency.

If this interpretation is correct, then the observed beat should be removed by increasing the scanning frequency (as illustrated later with Figs. 8 and 9) or by slowing the potential change. This was done by studying fibers under voltage clamp.

One experiment is illustrated in Fig. 3. The cell was held at −80 mV and depolarized by trains of pulses. These pulses, individually represented in the black trace in the inset in Fig. 3 B, had a triangular shape with an

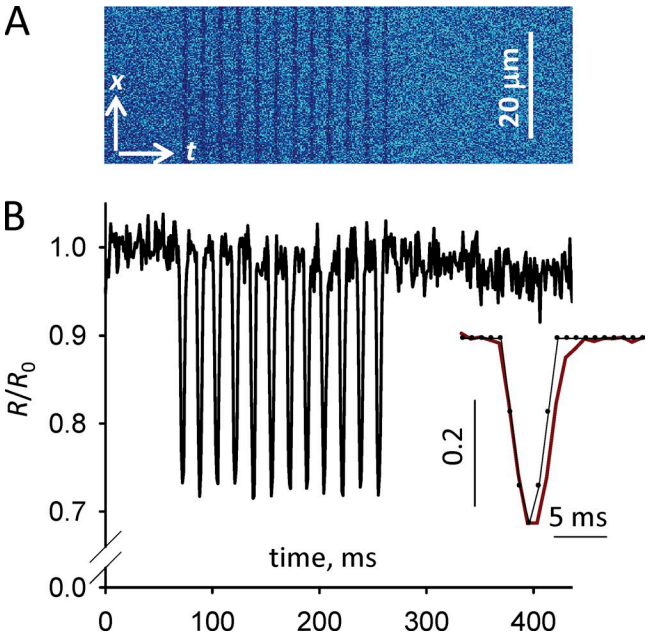

Figure 3. The di-8-ANEPPS signal elicited by trains of depolarizing pulses. (A) Average of four line scan images $F_{22}(x,t)$, obtained in a stained voltage-clamped fiber and corrected as described for Fig. 2 B. The fiber was held at −80 mV, and a train of 12 pulses (to +40 mV) was applied at a frequency of 60 Hz. The trains were repeated at 2-s intervals during 3 min. (B) The average SEER ratio $R(t)$. Ratio traces were calculated as described in Fig. 2 from four individual images, obtained at times of 0, 1, 2, and 3 min, and averaged. The individual $R(t)$ were similar to one another. (inset) Dark red trace, average of all transients in $R(t)$. Black trace, command potential of individual depolarizing pulses, scaled to match the experimental record. Dots plot individual values of the command, which was updated at 1-ms intervals. ID: 111011a_23, _25, _27, and _28.

amplitude of 120 mV and a duration at half magnitude of 3 ms. The depolarization frequency within the train was 60 per second (each train of 12 pulses lasted 200 ms).

To allow for signal averaging and to test the stability of the signal, the trains were repeated at 2-s intervals, without interruption, for 3 min. Line scan images of fluorescence F_{22} and F_{11} were acquired for the first train, and after 1, 2, and 3 min of application of this pattern. No change in the response was found in the four acquired images; there was no visible degradation of the signal after 3 min of application of this pattern.

Fig. 3 A displays the average of the four line scan images $F_{22}(x,t)$. The SEER ratio R (t), calculated for individual images as described for Fig. 2 and averaged over the four sets of images, is plotted in Fig. 3 B. The magnitude of the peaks was steady during the train. The "beat" visible under action potential stimulation was no longer present, in averages or individual images, when cells were subjected to these slower trains of depolarizations.

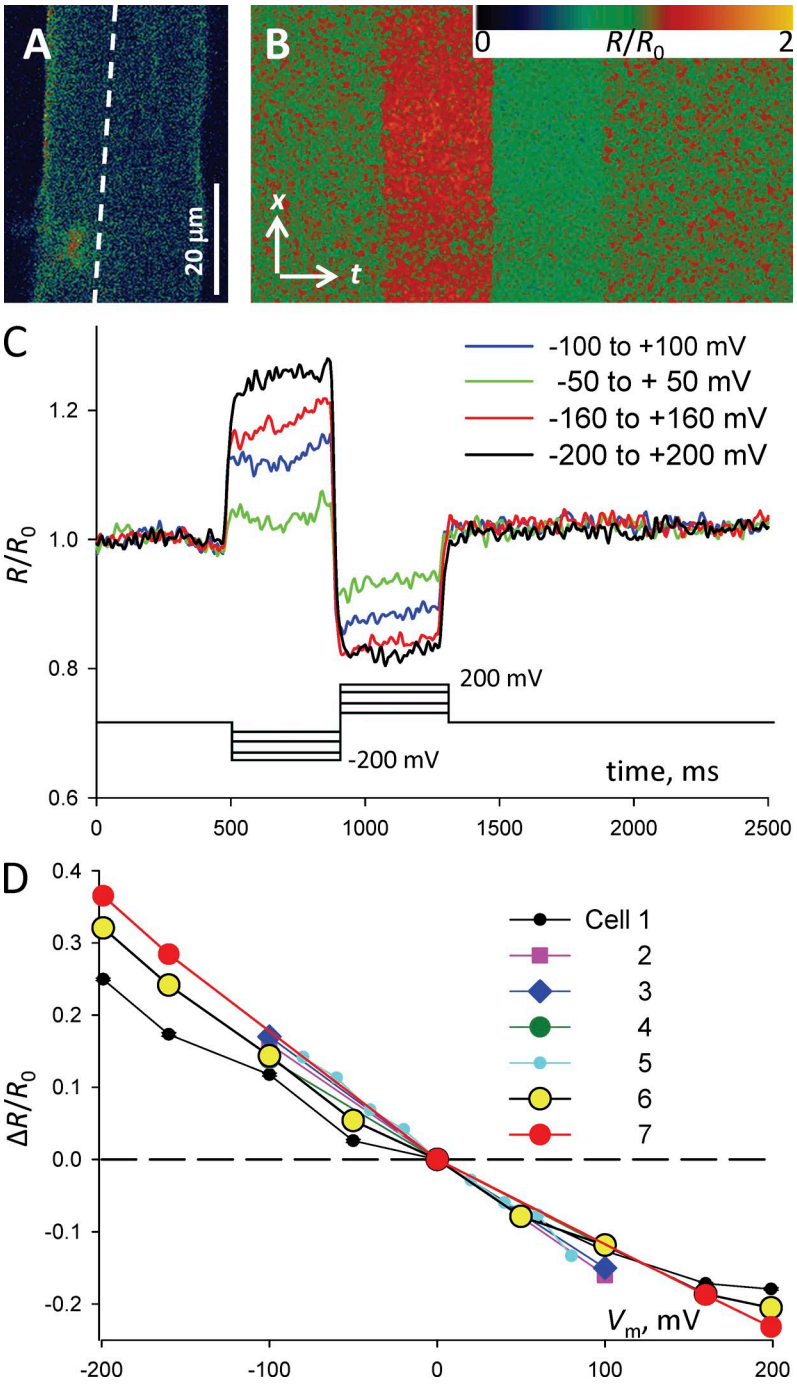

Figure 4. The steady SEER signal of di-8-ANEPPS under voltage clamp. (A) $F_{22}(x,y)$, indicating the scanned line (broken line) in a cell under voltage clamp held at 0 mV. (B) SEER ratio image $R(x,t)$, normalized to its resting value $R_0(x)$, when the cell in A was subjected to a biphasic pulse consisting of hyperpolarization to −160 mV for 400 ms followed by depolarization to +160 mV, as illustrated in C. (C) Line averages $(R(t)/R_0)$ in the same cell, subjected to the biphasic pulses levels coded by color. (D) Average level of R/R_0 during the pulse in the cell of A–C (black circles) and six others. The average slope was -0.15 $(100\ \text{mV})^{-1}$, with a standard deviation of 0.017. ID of cells 1–7: 091412a, -b, -c, -d, 111011a, 091712b, and 091712a.

The experiment also provided a first calibration of the signals. The average amplitude of the ratio change, $|\Delta R|/R_0$, was 0.258, which by Eq. 5 corresponds to S_L = 0.215 $(100\ mV)^{-1}$.

The dark red trace in Fig. 3 (inset) shows the average of the response to all 12 pulses, superimposed on the command potential (black). The dye signal follows the command potential with some delay. Because these probes are sufficiently fast to track an action potential (Montana et al., 1989; DiFranco et al., 2005), the error is likely caused by lags in the voltage change in response to the command, estimated at up to 0.7 ms in a patch voltage clamp of FDB cells at room temperature (Pouvreau et al., 2004).

The SEER signal of di-8-ANEPPS was also calibrated with long-lasting voltage clamp pulses, in experiments illustrated in Fig. 4. Fig. 4 A shows an image $F_{22}(x,y)$ of a stained cell held at 0 mV, and Fig. 4 B shows the SEER ratio $R(t)/R_0$ in a line scan along the dashed line in Fig. 4 A, upon application of a biphasic pulse of −160 mV and 400 ms duration in each phase. Plotted in Fig. 4 C are line averages of single SEER ratio images, taken while applying voltage clamp pulses as indicated. Fig. 4 D plots with black circles the average changes in R/R_0 during the pulses versus the applied voltage.

In the −100 to 100 mV region, the dependence is well described by a straight line through the origin. At greater separations from 0 mV, the dependence changes slightly, becoming steeper at large negative voltages and shallower at large positive voltages. In some cases, including the example, a slow drift was observed in the signals, resulting in a slight positive increase of the ratio after the end of the biphasic pulse. This shift subsided within seconds.

A similar study, with different ranges and increments of applied pulses, was performed in seven cells. The (minus) slope of the best fit linear function in the range of −100 mV to 100 mV, which according to Eq. 5 is equal to S_L, was on average 0.155 $(100\ mV)^{-1}$ (standard deviation of 0.017 and a range of 0.13–0.18).

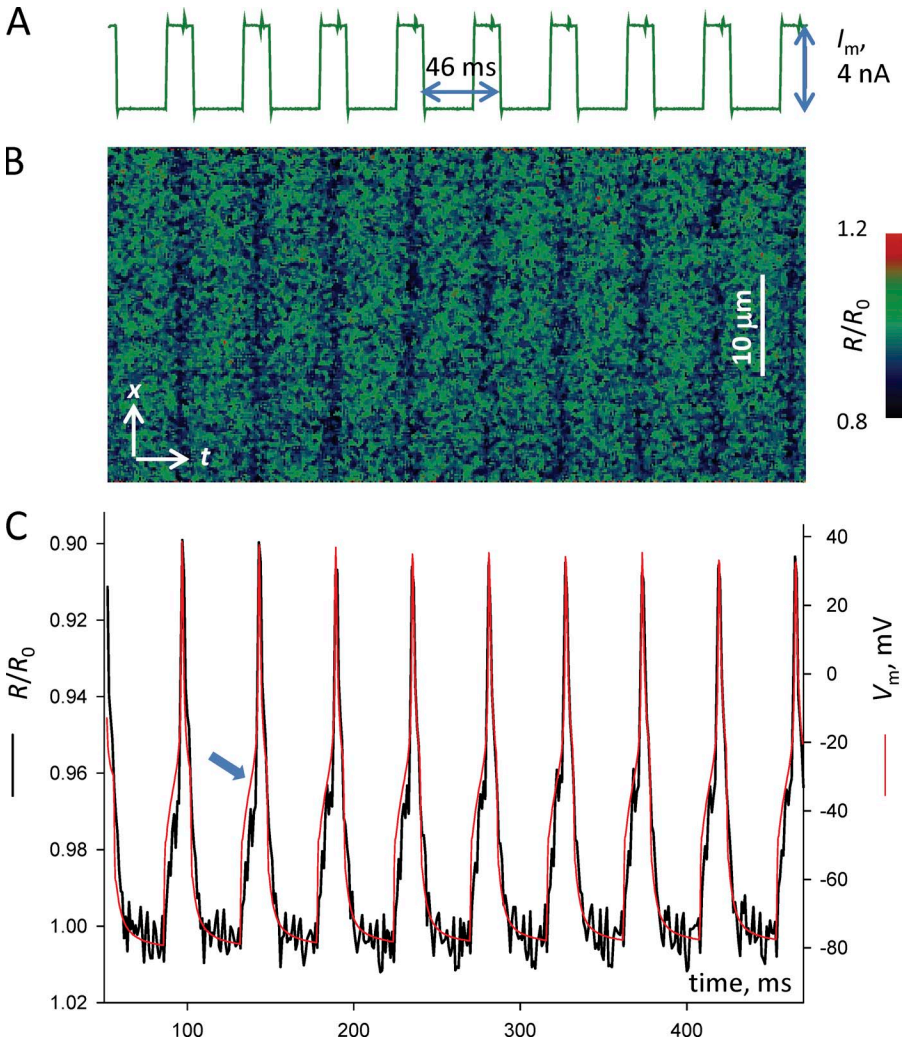

Figure 5. Membrane voltage, measured optically and with an intracellular microelectrode. The cell, stained with di-8-ANEPPS, was held under current clamp, at a pipette voltage of −80 mV, using the "silicone-clamp" technique. The active (grease-free) segment of the cell had a length of ∼100 µm and a diameter of 41 µm. The pipette had a resistance of 1.8 MΩ in the bath. (A) Measured current, I_m, for a nominal train of 40 nA pulses. (B) SEER ratio $R(x,t)/R_0(x)$, averaged over 16 trains. (C) Line-averaged R/R_0 (black trace) and simultaneously recorded pipette voltage V_m. Both records were plotted at vertical scales adequate to match the peaks. Note the discrepancy (arrow) reproducible with every pulse of the train. ID: 010712a, series 17–33.

An alternative calibration, which also provided a direct check of the kinetic properties of the monitor, was done by recording the SEER signal of di-8-ANEPPS in cells producing action potentials, which were simultaneously recorded with an intracellular electrode. An example is illustrated in Figs. 5 and 6. A piece of a stained cell was voltage clamped using the "silicone clamp" technique (Jacquemond, 1997). The cell was first covered with silicone grease, leaving a 100-µm segment free, and impaled with a pipette, containing an internal solution close to physiological conditions, within the silicone-covered region, ~150 µm away from the free region. Then, current-clamp mode was established and depolarizing current pulses were passed to elicit action potentials while measuring pipette voltage V_m. In the example, pulses of 4 nA, lasting 16 ms, were superimposed on a small holding current at a frequency of $(46\ \text{ms})^{-1}$. Fig. 5 A plots the applied current, I_m. In Fig. 5 B is the SEER ratio image $R(x,t)$, normalized to its value at rest, and averaged over 16 similar trains. The graph in Fig. 5 C plots ratio averaged over the scanned line (black) and the measured V_m (red). The vertical scales of R and V_m are chosen to approximately match the peaks.

As shown, the agreement between the optical signal and the directly measured pipette voltage seems good, except for a faster rise of V_m during the "shoulder" produced by the stimulus current (Fig. 5 C, arrow). In Fig. 6 B, where the same variables are plotted on an expanded time scale, the mismatch is seen to be caused by a rapid rise in the electric signal (arrow), cotemporal with the leading edge of the applied current (Fig. 6 A). This difference is due to series resistance error in the measured V_m. As shown in Fig. 6 C, a much improved agreement is found between the optical signal and the electric record digitally corrected by subtracting the product of I_m and a series resistance of 5.1 MΩ (contributed by the electrode and the inert segment of fiber between impalement point and end of the silicone cover). After correction, the scaling factor needed to match the two signals (i.e., S_L) was 0.113 $(100\ \text{mV})^{-1}$.

A final estimate of sensitivity is provided by the signal in Fig. 2 E, where peak $|\Delta R|/R_0$ is 0.33, assuming an action potential amplitude of 120 mV, S_L = 0.27 $(100\ \text{mV})^{-1}$. The various estimates derived from the present data therefore span a greater than twofold range, between 0.11 and 0.27 $(100\ \text{mV})^{-1}$. Variability in different tests and preparations is a known shortcoming of these dyes. Reasons, which are explored further in the next subsection, include sensitivity to the membrane dipole potential (Gross et al., 1994; Vitha and Clarke, 2007), which makes the signal sensitive to the local composition of the membrane, and the progressive internalization and redistribution of the dye, which causes sensitivity to decay with time. Accurate interpretation of the signals therefore requires contemporary calibrations in the same cells (Zhang et al., 1998; DiFranco et al., 2011).

It should be noted that in the experiments with the SP2 scanner, S_L is not at its optimum. Fig. 1 B shows that a substantial improvement would be achieved by using Ex1 405 nm (a laser line not available in this scanner) instead of 458 nm. Indeed, the excitation efficiency at 405 nm nearly doubles upon depolarization, a factor that affects $S_{L,\,ex}$ and, through it, S_L, as described by Eq. 4. This excitation light was used to advantage in a second implementation of the SEER technique, presented later.

Factors that condition sensitivity

The greater than twofold variability in sensitivity may be caused by many factors. We explored two of them, passage of time and intensity of staining, with observations illustrated in Fig. 7. Fig. 7 A illustrates the effect of time after the establishment of whole-cell clamp in a cell held at 0 mV. A general functional stability of the cell is

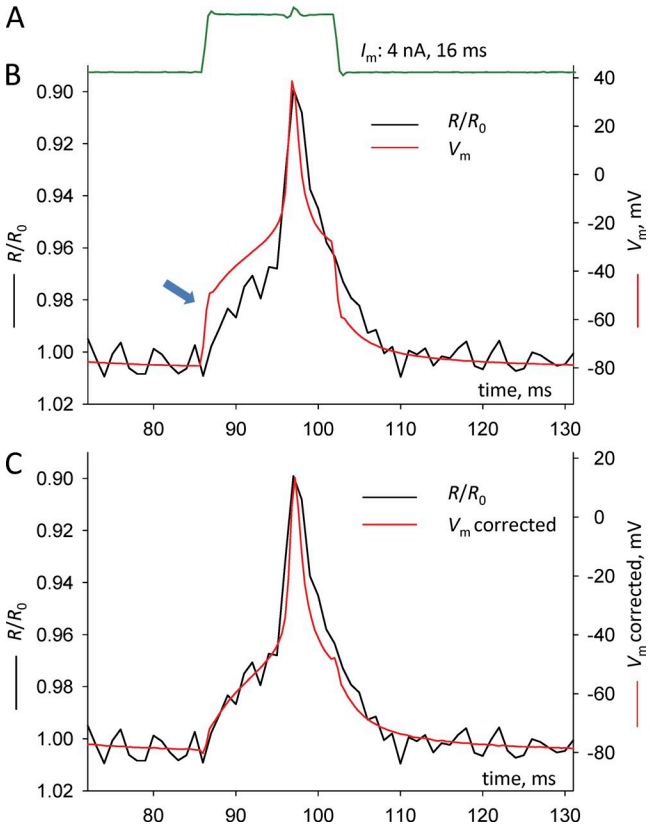

Figure 6. Membrane voltage, corrected for series resistance. (A) Recorded current pulse during the train in Fig. 5. (B) Detail of R/R_0 and V_m from the plots in Fig. 5 C, at an expanded time scale, to show the systematic difference between electric and optical records. (C) R/R_0 plot from B (black) and the sum (V_m corrected) of V_m and I_m multiplied by a factor (−5.1 MΩ) that optimizes the overlap. Note the change, introduced to maintain overlap, in the scale of V_m corrected. The ratio of the two vertical scales in C, ~0.1 $(100\ \text{mV})^{-1}$, is equal to the sensitivity S_L.

indicated by the constancy of linear membrane capacitance at 1.9 nF. The individual averages of fluorescence F_{22} and F_{11} were fairly constant during this time, and are not shown. The plot with blue squares represents R at the holding potential as a function of time after the whole-cell clamp. As can be seen, R was initially constant and then increased slightly. In seven cells studied, the ratio stayed within 20% of the initial value when the fiber was kept depolarized.

The value of R during a pulse to −100 mV, applied at different times, is plotted with black circles (Fig. 7). The relative value of the ratio, that is, the quotient $R(-100\text{ mV})/R(0\text{ mV})$, plotted in red in Fig. 7, decayed from an initial value of 1.2 to 1.16 by 12 min and 1.08 by 25 min. This was also a reproducible observation; in the cells studied the relative change in ratio, $\Delta R/R_0$, was reduced by 10 to 25% after 15 min.

In Fig. 7 B, the sensitivity measured in the experiments illustrated in Fig. 4 C is plotted versus the "invariant," a linear combination of F_{22} and F_{11} that is insensitive to V_m and is therefore proportional to the concentration of dye in the scanned region (see "Additional methods"; Launikonis et al., 2005). As shown, the sensitivity appears to decay as [dye] increases. The Pearson correlation coefficient r was −0.64 ($r^2 = 0.41$). This sample value was used to test the hypothesis of no correlation ($\rho = 0$) either by means of the statistic

$$w = \sqrt{n}\,\frac{r^2}{1+r^2} = 1.84$$

or the statistic

$$z \equiv \sqrt{\frac{n-3}{4}}\log\frac{1+r}{1-r} = 1.51,$$

both of which have normal distribution, with mean 0 and standard deviation 1, in the hypothesis of no correlation (Cramér, 1946). Neither statistic reaches the critical confidence level for rejecting the null hypothesis; thus, there was no significant evidence of a link between sensitivity and staining density. The relatively high values of these statistical measures of correlation, however, suggest that dense staining may result in lower sensitivity.

SEER of di-8-ANEPPS at high temporal resolution

SEER is analogous to excitation ratioing in requiring the alternating use of two light sources. In this regard it shares with all excitation ratioing procedures the disadvantage of a temporal resolution reduced by half. The highest line scanning frequency that the SP2 AOBS provides, 2 kHz, is thus reduced to an effective maximum of 1 kHz. This rate is not sufficient to monitor the higher frequency components in action potentials, explaining the observed beats (Fig. 2).

The problem is entirely circumvented using a faster scanner. Here we illustrate the implementation of the technique using the 5 LIVE slit scanner. The maximum line-scanning frequency of this device when alternating excitation light is 16 kHz, which results in a SEER acquisition frequency of 8 kHz. Fig. 8 A shows a SEER ratio image obtained in the same way as in Fig. 2 A, from a cell paced at 50 Hz. The beat between successive action potentials is no longer present. In Fig. 8 B are individual fluorescence transients, $F_{11}(t)$, $F_{12}(t)$, $F_{21}(t)$, and $F_{22}(t)$, obtained at wavelengths detailed with Fig. 1 B, averaged over 10 action potentials and normalized to their initial value. In Fig. 8 C are the three possible ratios that include F_{22}. Similar to the study with the pinhole scanner, illustrated in Fig. 2, the SEER ratio (F_{22}/F_{11}) had greater signal amplitude than both the emission and excitation ratios. An additional advantage of the high rate at which the two excitation lights were alternated (and data were acquired) was to increase the rejection of movement artifact much more effectively than with the SP2 scanner.

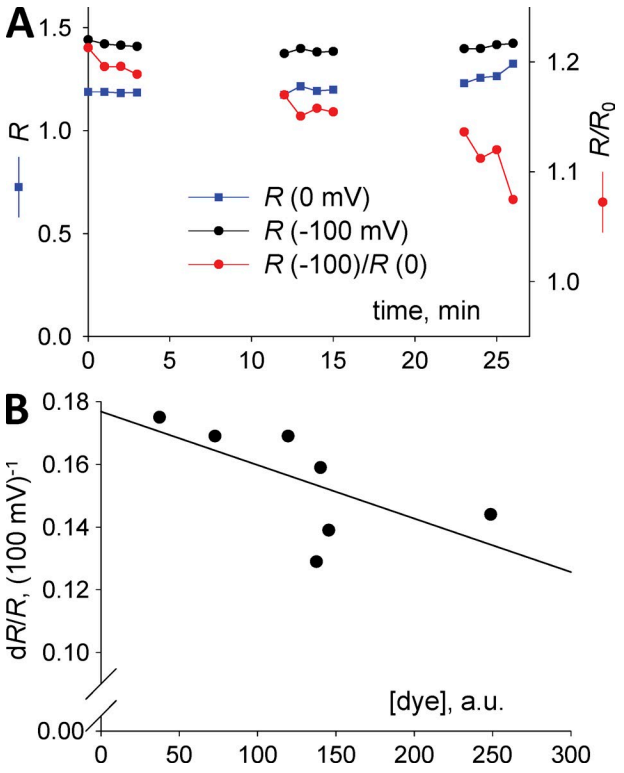

Figure 7. Factors affecting sensitivity. A stained cell was held at 0 mV and the SEER di-8-ANEPPS signal was monitored intermittently. (A) Line-averaged R (F_{22}/F_{11}, blue) increases slightly with time during the experiment. R/R_0 during a pulse to –100 mV (red) decays in repeated pulses, so that by 25 min S_L is reduced by 50% of its initial value. (B) S_L in the cells of Fig. 4 C versus the invariant combination of F_{22} and F_{11} that is proportional to the concentration of dye (labeled [dye]). The correlation coefficient r^2 was 0.41. ID: 091412a, series 10–76.

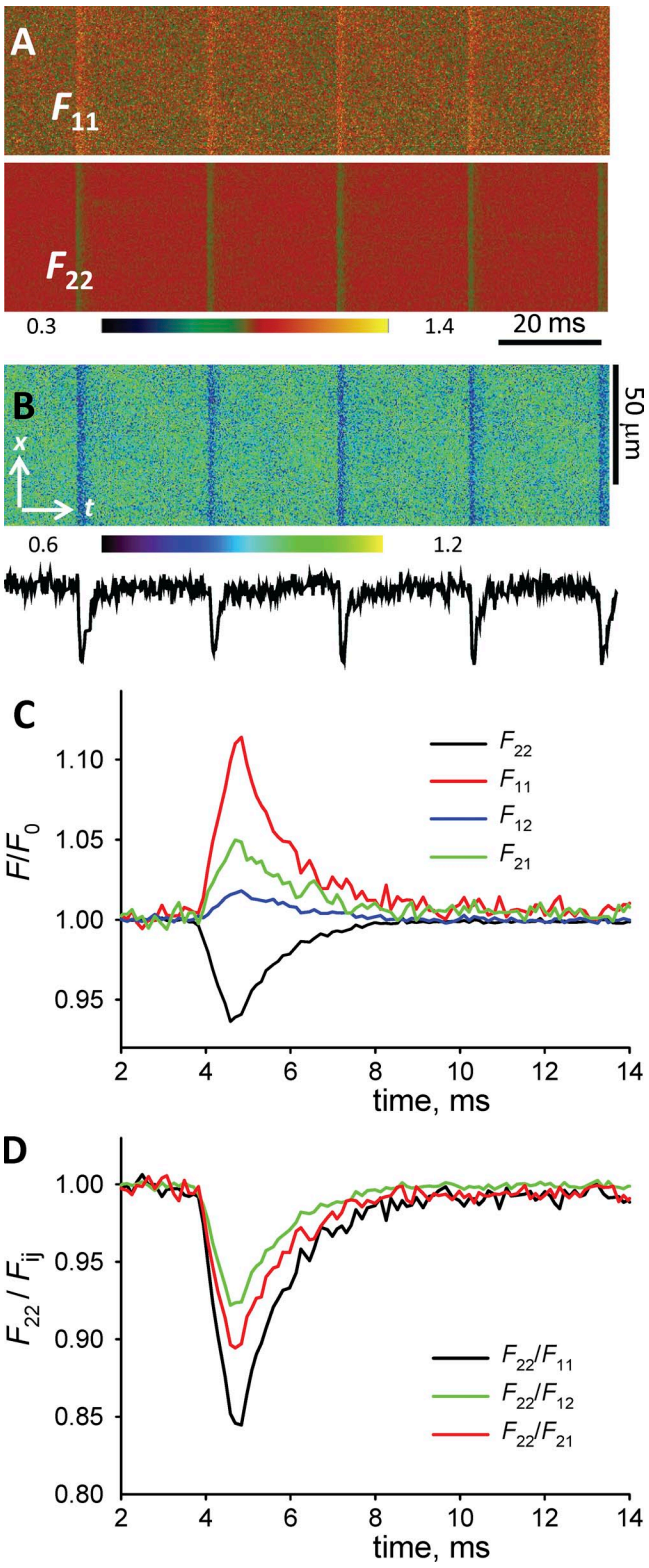

Figure 8. Signals of di-8-ANEPPS at high temporal resolution. The stained cell, generating action potentials under field stimulation, was line-scanned in a 5 LIVE slit scanner with line-interleaved excitation for an effective ratiometric frequency of 8 kHz. (A) Images $F_{11}(x,t)$ and $F_{22}(x,t)$ (averages of four individual line scans) obtained with protocols illustrated in Fig. 1 and normalized (here and in the other panels of this figure) by the corresponding baseline averages $F_{11}(x,0)$ and $F_{22}(x,0)$. (B) The SEER ratio $R(x,t)$ of the images in A and its line average $R(t)$ (black trace). (C) Line-averaged fluorescence transients, $F_{11}(t)$, $F_{12}(t)$, $F_{21}(t)$, and $F_{22}(t)$, obtained at wavelengths detailed with Fig. 1, averaged over 10 action potentials and normalized to their initial value. (D) The three possible ratios that include F_{22}. Note that the SEER ratio (F_{22}/F_{11}) reaches the greatest amplitude. ID: 091912a_46 series 46.

This implementation had one major disadvantage: in the example shown, the amplitude of the fluorescence changes was at most 0.11 F_0 (it reached up to 0.12 F_0 in other experiments) and that of the ratio signals was 0.11 R_0 (which was the maximum observed with this implementation). This reduction, to 50–70% of the dynamic range achieved in the SP2 system, is due to the fact that the 5 LIVE scanner uses fixed optical components and therefore has less freedom to select emitted light (compare the description of methods in reference to Fig. 1).

A calibration under voltage clamp is illustrated in Fig. 9. As done with the pinhole scanner and illustrated in Fig. 4, a stained cell was subjected to biphasic voltage clamp pulses from a holding potential of 0 mV while scanning along a line parallel to the fiber axis. Fig. 9 A shows the line scan ratio images at various voltages. Fig. 9 B shows the line-averaged ratio ($R(t)/R_0$) and Fig. 9 C shows its mean after the record settles, plotted versus the applied voltage. Again, the dependence is nearly linear, with slope of -0.10 $(100\ \text{mV})^{-1}$ between -100 and +100 mV.

Applications to questions of muscle physiology

In the following sections we demonstrate the use of this technique to explore two topics of muscle physiology. Given its high sensitivity, the implementation using the SP2 pinhole scanner was found to be useful to detect early electrophysiological changes associated with muscle fatigue. The second implementation, with its greater temporal resolution, was able to evaluate lags in propagation of action potentials to the cell interior along the t system.

Cellular determinants of muscle fatigue. It is believed that the cellular mechanisms leading to muscle fatigue include changes in the rapid Ca^{2+} movements of excitation–contraction coupling, in turn caused by redistribution of the calcium originally stored inside the sarcoplasmic reticulum (e.g., Allen et al., 2011). However, persistent activation at high frequency is known to result in alterations or failure of action potentials (for review see Allen et al., 2008). We used SEER signals of di-8-ANEPPS to determine whether specific stimulation patterns that lead to reduction in

contractile tension cause significant changes in the action potential.

An experiment using the pinhole SP2 system is illustrated in Fig. 10. The enzymatically isolated fiber was

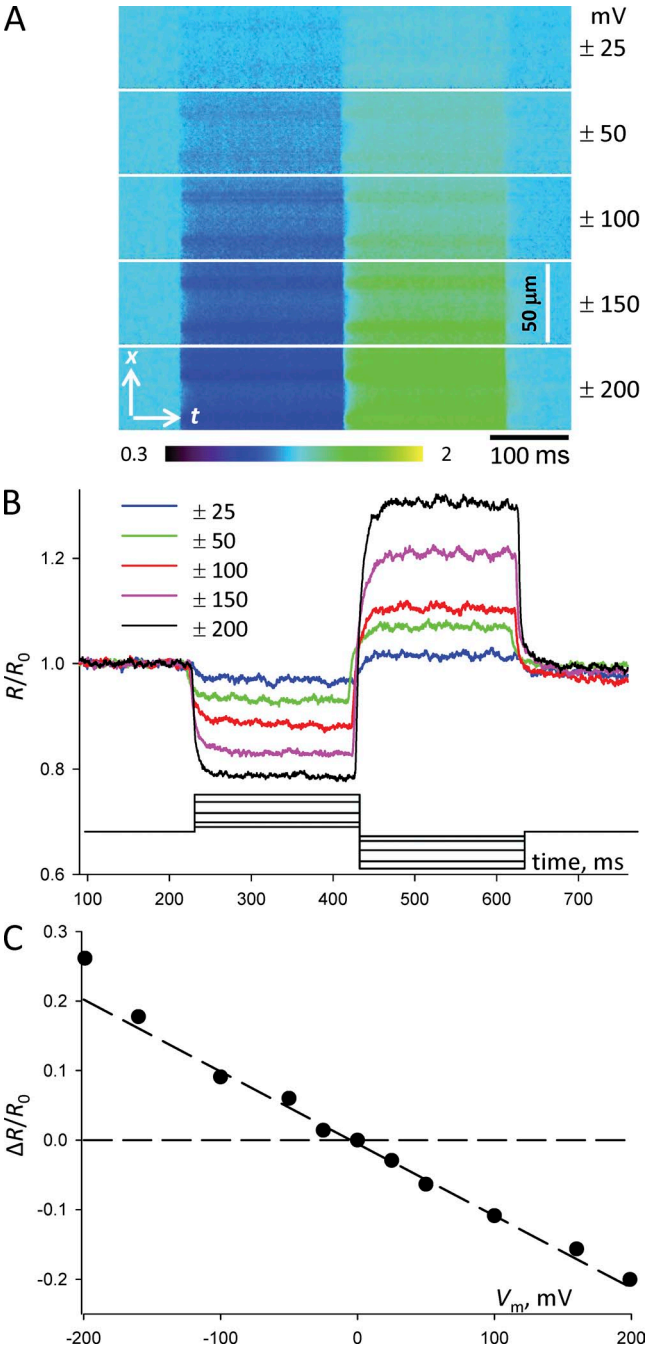

Figure 9. Calibration of SEER signals at high temporal resolution. A stained cell held at 0 mV under voltage clamp was subjected to biphasic pulses of 400 ms illustrated in B, and line scanned as in Fig. 8. (A) SEER ratio images $R(x,t)$ for five pulse amplitudes. (B) Line-averaged, normalized ratio, $R(t)$, during the corresponding pulses. (C) $R(t)$, averaged during the last 150 ms of each pulse (a time when the transient had settled) versus the applied voltage. The line plots the best linear fit to all points between −100 mV and +100 mV; its slope is 0.103 $(100\ \text{mV})^{-1}$. ID: 091912a.

otherwise intact. The stimulation pattern, shown in the top left side of Fig. 10, consisted of tetanizing trains of stimuli at a frequency of 70 Hz, lasting 350 ms. These trains, one of which is shown in Fig. 10 A, were repeated at 2-s intervals. In separate experiments on whole FDB, we found that this pattern resulted in reduction of tetanic tension by 65% after 3 min. As stated for the experiment of Fig. 3, which applied a similar activation protocol under voltage clamp, there are no progressive changes in the dye signals upon long-lasting application of depolarizing pulse trains of constant voltage. Any alterations in the signal should therefore correspond to changes in the action potentials.

Fig. 10 (A–C) shows $R(t)$ records at the beginning (black), after 1 min (blue), and after 3 min of uninterrupted application of trains of stimuli (red). The signals in Fig. 10 A were fairly regular; they were somewhat altered after 1 min and severely reduced after 3 min. As shown by Fig. 10 D obtained after 10 min of rest (green), the alteration was fully reversible. (The individual downward signals should not be taken as proportional indicators of action potential amplitude, as the traces plot line averages, and therefore a reduction of the peak difference may reflect changes in amplitude or local failure of the action potential, which is visible on the fluorescence images, as in panel c).

Variable degrees of alteration were found in >20 cells studied similarly. In contrast, no significant changes in the dye signal were found when the frequency of stimuli within the train was 40 Hz, provided that the duration of the trains was 350 ms or less. Again, in separate experiments on whole FDB, we found that 3 min of a stimulus protocol with these characteristics also depresses contractile force substantially, by 47% of the initial tension (at both 40 and 70 Hz). The integrity of the action potential under these conditions points to alterations downstream of the excitation and voltage-sensing steps, including Ca^{2+} movements, as causes of the reduction in force.

Simultaneous recording of action potentials at variable depth. SEER of di-8-ANEPPS fluorescence at the high temporal resolution afforded by the slit scanner can be used to compare properties of the change in voltage at different distances from the plasma membrane, as illustrated in Fig. 11. Fig. 11 A shows a stained cell placed at a convenient 20° angle with the horizontal, which is also the position of the scanning line (broken line). The extent of the line comprised inside the cell is marked in Fig. 11 A with a horizontal segment. Fig. 11 B shows the line scan image of the SEER ratio. The cell was paced at 50 Hz with field pulses of 0.2 ms. A large transient signal reflecting these pulses (up-going on the top side of the fiber, facing the field cathode) is visible in the ratio image. Fig. 11 C shows line averages $R(t)/R_0$; shown in black trace is the average in a superficial region

of the cell (marked by the black bracket in Fig. 11 B). In green trace is the average in the axial region marked by the green bracket. In red trace is the ratio record in the central region, scaled to match the peak of the record from the surface. The difference between the nadirs of both records is 0.41 ms. As shown in Fig. 11 A, the length of the region scanned inside the cell is 107.6 μm (a length that multiplied by the cosine of the angle formed with the cell axis yields the cell diameter, 36.8 μm). If we interpret the delay between nadirs as the time required for propagation of the electric response, a speed of propagation can be calculated. Assuming for simplicity that activation of the whole surface occurs simultaneously, the propagation can be modeled to proceed in an axisymmetrical manner. The effective or average distance that the propagating action potential must traverse under this hypothesis is marked by the gray vertical segment labeled Δx in Fig. 11 B (which spans the distance from the center of the surface region (black bracket) to the top quartile (middle of the top half) of the center region (green bracket). This distance, 37.5 μm along the scanned line, corresponds to 12.7 μm on a perpendicular to the fiber axis. If the propagation time is measured by the lag in the arrival of the nadir of the optical signal, the speed is 30.1 m/s.

The measurement is complicated by the presence of the prominent "artifact" associated with the applied field, which varies steeply with position in the scan. In spite of this limitation it is possible to compare the observed lag with estimates of propagation times obtained by other methods. For instance, DiFranco et al. (2005) applied voltage clamp pulses to a mouse cell stained with di-8-ANEPPS and immersed in Na^+-containing Tyrode's solution. The di-8-ANEPPS signal, which largely reflected t system voltage, had an asymmetrical "positive" component upon application of depolarizing pulses.

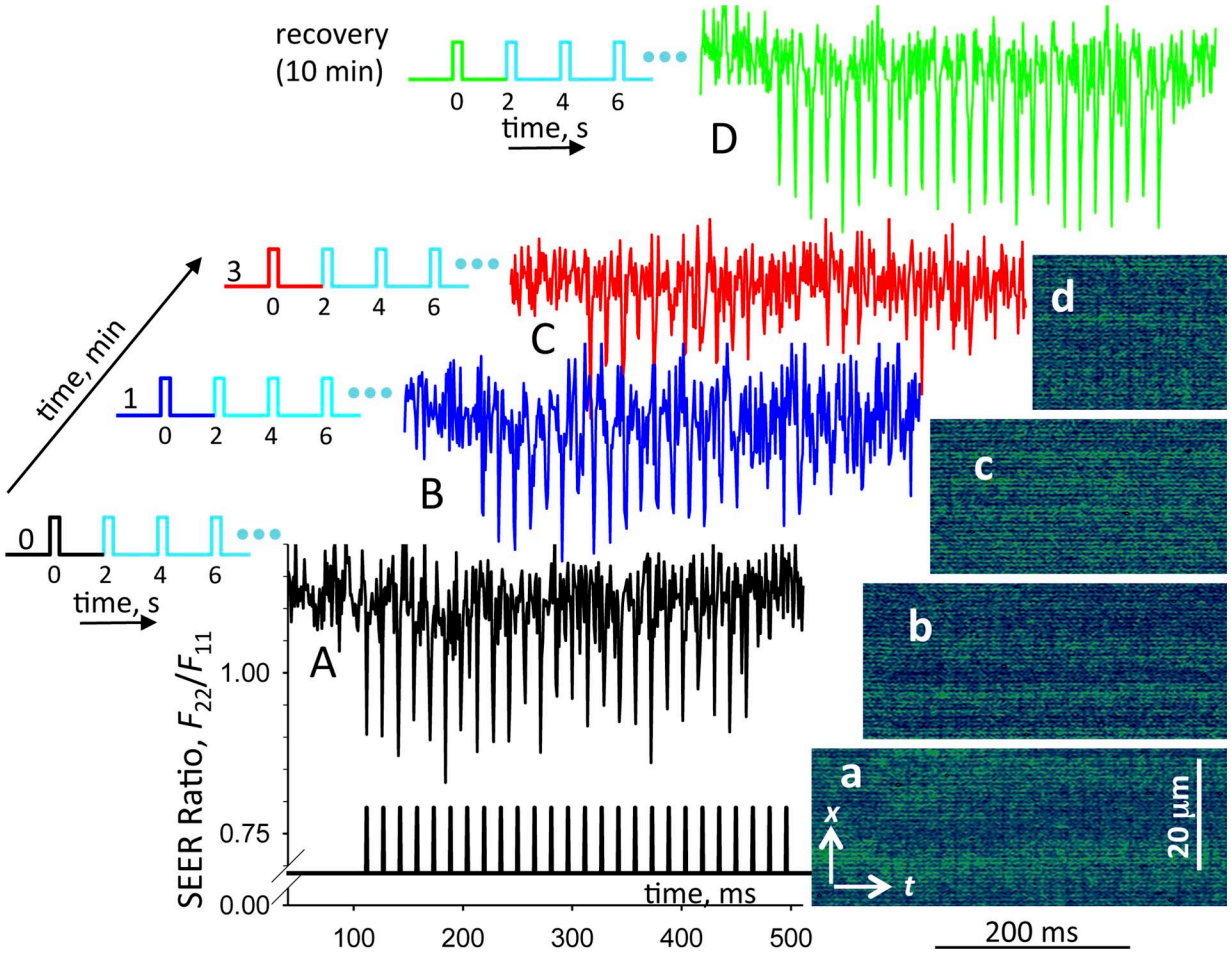

Figure 10. Claudication of the action potential during fatigue-inducing stimulation. SEER ratio $R(t)$ in a fiber subjected to the pattern of field stimuli represented at the top left. Plots labeled in upper-case letters are line averages of ratio images, sections of which are shown correspondingly labeled in lower-case letters. In the diagrams, rectangular depolarizing deflections represent trains of suprathreshold field stimuli at 70 Hz, one of which is plotted on A (bottom). The trains lasted 350 ms and were applied continuously at 2-s intervals. (A, a) $R(t)$ and image upon the first application of the train. (B, b) The application at 1 min. (C, c) Application at 3 min. Note the alterations in signal pattern, including lower amplitude, and spatially inhomogeneous transients. (D, d) Recovery run, 10 min after stopping the stimuli. ID: 111511b_12_13_15_17.

This was interpreted as reflecting a propagating action potential, escaping from the voltage-clamped plasma membrane. Its temporal properties (Fig. 7 B of DiFranco et al., 2005) were not unlike those of the "center" signal in Fig. 11 C. Notably, the peak of the signal occurred 0.3 ms after the leading edge of the depolarizing pulse.

DISCUSSION

After its introduction as a means to enhance ratiometric measures of intra-SR [Ca^{2+}], SEER was found to be useful for imaging [Ca^{2+}] with indo-1, and [H^+] with carboxy-SNARF, an application that permitted sensitive dynamic imaging of [H^+] in basophils (Musset et al., 2008) and neutrophils (Morgan et al., 2009). Launikonis et al. (2005) suggested two additional applications that have yet to be tested: measures with voltage sensors that accumulate in the mitochondrial matrix (including TMRE, TMRM, and rhodamine 123) and measures with fura-2, which in addition to its well-known excitation changes, features a blue shift in emission upon binding Ca^{2+}.

We now show that SEER is also able to increase the sensitivity of di-8-ANEPPS, a result implying that SEER will be applicable to other fast electrochromic voltage sensors.

As summarized in a review article by Sjulson and Miesenböck (2007), fast optical reporters of membrane voltage fall into four categories: fast synthetic dyes or VSDs (Cohen and Salzberg, 1978), two-component voltage sensors that operate by Förster resonance energy transfer (FRET; González and Tsien, 1995), hybrid biosynthetic protein-dye systems (Tsien and González, 2006; Chanda et al., 2005; Wang et al., 2010), and genetically encoded sensors (Siegel and Isacoff, 1997). Their relative merits and shortcomings are well known. With regard to strengths, biosensors

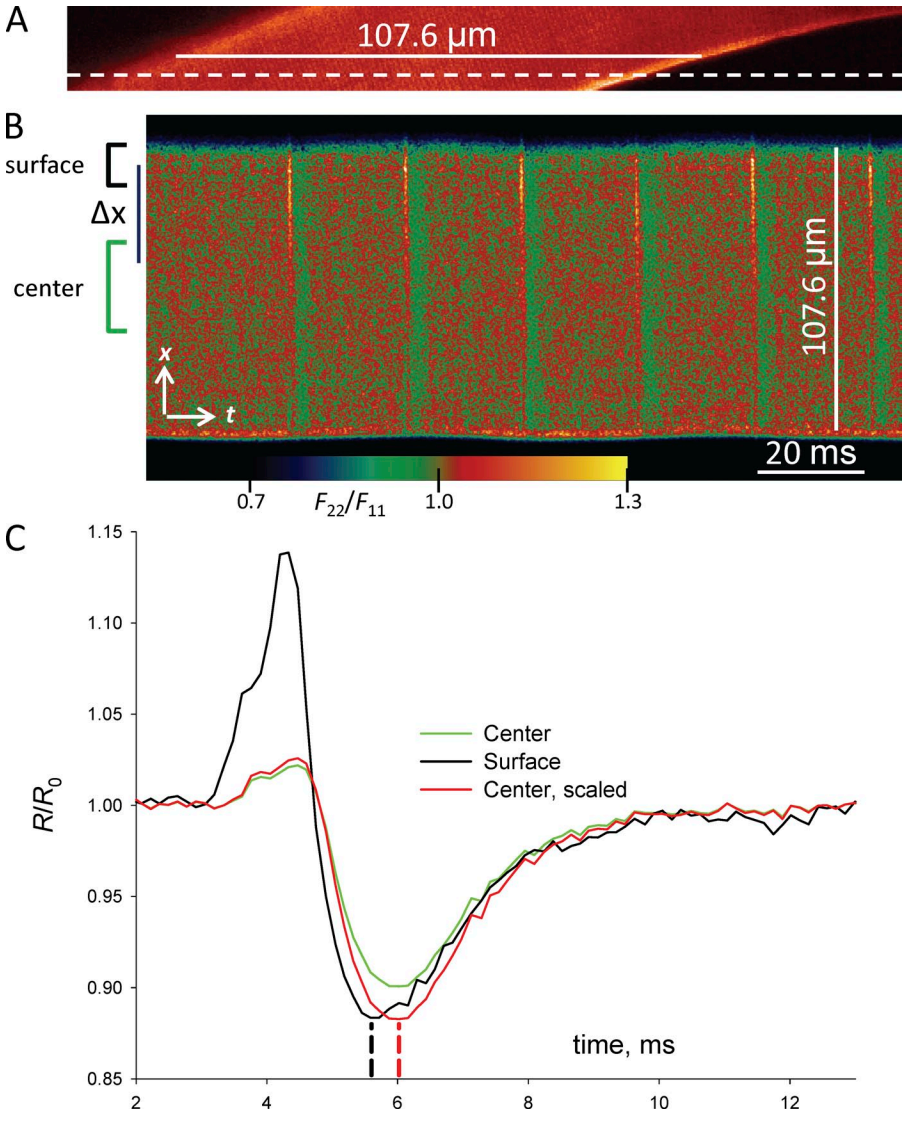

Figure 11. Simultaneous recording of action potentials at variable depth. (A) Stained cell placed at a 20° angle with the scanning line (broken line). The extent of the line comprised inside the cell is marked in A with a horizontal segment. The cell was paced at 50 Hz with field pulses of 0.2 ms. (B) Normalized SEER ratio image $R(x,t)$. (C) Average $R(t)$ over segments of the scanning line marked by color-coded brackets in B. In red trace is the ratio record in the central region (green), scaled to match peaks with the record from the surface (black). Note the lag between the nadirs of the two signals, interpreted in the text as reflecting a propagation speed of 30.1 m/s. ID: 082112, average of series 03–09.

promise and in some cases achieve selective targeting, whereas two-component VSDs and some hybrid systems are reported to achieve high sensitivity, with $\Delta F/F_0$ reaching values >0.5 $(100\ \text{mV})^{-1}$ in special cases (González and Tsien, 1997; Bradley et al., 2009). But biosensors are comparatively difficult to implement, suffer from low sensitivity and slower kinetics (imposed by their FRET mechanism) and may interfere with function. Two-component VSDs are simpler, but they also have kinetic limitations and their intramembrane mobile component imposes a capacitive current upon potential changes.

Single synthetic VSDs, however, continue to be valued for their simplicity, near-linearity in the voltage ranges of interest, and robust responses. Among them, di-8-ANEPPS is preferred for its better sensitivity and slower rate of internalization to cytosol and organelles, which also results in lower toxicity (Rohr and Salzberg, 1994). Here we have shown that a relatively simple technical change, SEER, improves the sensitivity of di-8-ANEPPS by close to twofold, to reach values as high as 0.27 $(100\ \text{mV})^{-1}$. We also argued that a simple change in the first implementation described above, the use of 405 nm as Ex1, should result in an additional near-doubling in sensitivity.

Although the improvement of performance of di-8-ANEPPS is significant and yields immediate benefits for the study of muscle function, a more transcendental implication of the present work is that the SEER approach can be applied to many other sensors. It is well suited for dyes that work by electrochromism, in which both emission and excitation spectra shift similarly. As discussed in the Theory section (Eq. 1), in these cases ratioing of fluorescence compounds by addition the intrinsic sensitivities of fluorescence in two spectral regions, and SEER provides a further improvement, close to twofold, over the individual sensitivities of emission or excitation ratioing.

This discussion implies that the SEER technique will further improve the performance of the better dyes. As an example of the values of sensitivity that can be reached, consider ANNINE-6, an anellated hemicyanine with the greatest reported electrochromic shifts that we have found (Hübener et al., 2003). Its response has been quantified in detail, so that it is possible to predict with precision its performance under SEER. Fig. 5 (bottom right panel) of Fromherz et al. (2008) maps its $\Delta F/F$ per unit voltage change as a function of both excitation (Ex) and emission (Em) wavelengths. The putative SEER application would use F_{11} excitation at 458 nm and emission near 530 nm. With these choices, $\Delta F_{11}/F_{11}(0)$ is $\sim$0.3 $(100\ \text{mV})^{-1}$. For F_{22}, SEER would be optimal with excitation at 488 nm and emission near 620 nm. With these choices, $\Delta F_{22}/F_{22}(0)$ would be -0.3 $(100\ \text{mV})^{-1}$. From these values and Eq. 5, a SEER sensitivity of 0.46 $(100\ \text{mV})^{-1}$ is derived as follows:

$$100\,\text{mV}\times S_L \equiv \frac{1}{R_0}\left|\frac{\Delta R}{\Delta V}\right| = \frac{F_{11}(0)}{F_{22}(0)}\left|\frac{F_{22}}{F_{11}} - \frac{F_{22}(0)}{F_{11}(0)}\right| =$$

$$\left|\frac{F_{22}/F_{22}(0)}{F_{11}/F_{11}(0)} - 1\right| = \left|\frac{0.7}{1.3} - 1\right| = 0.46$$

Two implementations of the technique were useful when applied to current physiological questions. Applied to fibers subjected to a fatiguing protocol of action potential stimulation, the technique evinced progressive deterioration of action potentials at the frequencies commonly used in this type of studies. The technique identified a lower stimulation frequency, 40 Hz, which did not significantly change the features of the action potentials at room temperature, while still causing fatigue. This less intense protocol will be useful to produce fatigue by mechanisms other than alterations of electrical excitability, and will therefore help in understanding these mechanisms.

Implemented on a fast slit-scanning confocal system, the technique was applied to produce what to our knowledge are the first simultaneous recordings of optical signals of membrane voltage at different depths in a skeletal muscle fiber. The technique clearly revealed lags in depolarization of deep regions of the t-tubular system, which is consistent with estimates obtained by other methods.

The technique has the drawbacks common to all excitation ratio methods. Because SEER requires alternating excitation lights, its temporal resolution is limited by the speed of excitation switching and is ideally implemented with acousto-optical filters and beam splitters. When not limited by light switching, the effective temporal resolution is one half of that of line acquisition. The 5 LIVE slit scanner has a nominal top speed of 66 kHz, which would result in an effective SEER frequency of 33 kHz. In our experience, however, the highest frequency that yielded consistent results when alternating excitation lasers was 16 kHz, resulting in an effective SEER frequency of 8 kHz, reached in the experiments demonstrated here. There are other commercial scanners with comparable sampling rates. Among those, the SP8 (Leica) has the highest nominal rate, 24 kHz, which should produce SEER line scans at 12 kHz. This device offers spectral definition of emitted wavelengths, and hence it should yield the high sensitivity found with the SP2 scanner. Implemented with laser lines at 405 nm and 514 nm, SEER of di-8-ANEPPS with the SP8 should reach a sensitivity near 0.35 $(100\ \text{mV})^{-1}$.

Other drawbacks were noted with this technique: the signal decayed markedly with the time elapsed after staining, probably due to internalization of the dye. Additionally, we found a mild negative association between density of staining and sensitivity, which could be due in part to a greater internalization of the dye when staining

is higher, and a large variation in sensitivity among different cells, which could obey to different causes, including variable membrane composition and elapsed time. These drawbacks, common and usually more marked with other electrochromic dyes, are intrinsic to the use of di-8-ANEPPS with or without the SEER technique.

In conclusion, ratioing of signals obtained with different wavelength protocols was shown to increase the sensitivity of the membrane voltage monitor di-8-ANEPPS, as well as to reduce the susceptibility to common-mode interferences. The use of SEER was shown to increase the sensitivity further, nearly doubling it relative to conventional excitation or emission ratioing. The actual values of sensitivity demonstrated here varied between 0.1 and 0.27 $(100\ \text{mV})^{-1}$, a variability that is caused by decay with elapsed time, among other causes. Under conditions of excitation and emission available with other commercial scanners, SEER of di-8-ANEPPS should reach a sensitivity of 0.35 $(100\ \text{mV})^{-1}$ or greater. Other dyes with published spectra should top 0.45 $(100\ \text{mV})^{-1}$. Two implementations of the technique had different virtues and drawbacks: a conventional pinhole scanner with spectral definition of fluorescence emission ranges allowed for greatest sensitivity, whereas a fast slit scanner yielded temporal resolution adequate for detailed monitoring of action potentials. By imaging with the conventional pinhole scanner during repeated stimulation, we demonstrated severe decay and local failing of action potentials upon stimulating protocols commonly used in studies of the mechanisms of fatigue. Using the fast slit scanner, we were able to monitor the action potential propagating inwardly along the t system. These examples add membrane voltage to the growing number of dynamic measurements that can be enhanced with the use of SEER.

ADDITIONAL METHODS

Protocols using mice were approved by the Institutional Animal Care and Use Committee of Rush University, which found them consistent with their ethical standards. Results were collected from 25 mice (*Mus musculus*; Swiss Webster). The animals were killed by CO_2 inhalation. Procedures for dissection and dissociation of cells were as described by Royer et al. (2008). Experiments were performed at 20–22°C.

A unique identifier ID in the form of MMDDYYa_nnn is provided in the figure legends for each set of data illustrated. The first six digits provide the date, the following letter (a) identifies the experiment/cell, and the next three digits (nnn) give the image or image series shown in the figure.

Optical methods and electrophysiology

Isolated cells were studied in a plastic chamber with a 0.17-µm glass coverslip bottom mounted on a confocal microscope (SP2 AOBS [Leica] or the 5 LIVE component of an LSM 5 Duo microscope [Carl Zeiss]), where they were stained by 30 min of exposure to saline with 5 µM di-8-ANEPPS and 0.25% Pluronic F-127 in DMSO. They were either field stimulated at supramaximal voltages through platinum electrodes or patched near their center and clamped at −80 mV (details described by Royer et al., 2008). Line scan images $F(x,t)$ of fluorescence of di-8-ANEPPS, such as those in Figs. 2 and 4, were corrected for bleaching and for inhomogeneities of staining. The correction for bleaching consisted of division by function $F_{b,n}(t)$, defined as

$$F_{b,n}(t) \equiv \frac{F_b(t)}{\int_0^{t\max} F_b(t)},$$

with $F_b(t)$ representing the spatial average of the line scan fluorescence $F_b(x,t)$ imaged in the absence of voltage changes. The correction for staining inhomogeneity consisted of division by the function $F_0(x)$, an average of $F(x,t)$ over the time before the voltage changes. Line averages of fluorescence, $F(t)$, such as those in Fig. 2 B, were obtained by averaging over x line scans $F(x,t)$ corrected for background, bleaching, and staining inhomogeneity. Ratios, $R(x,t)$, which could be "emission," "excitation," or SEER, were line-averaged to yield $R(t)$. The result was similar but not identical when $R(t)$ was calculated by ratioing line-averaged fluorescence records, $F(t)$. An alternative $R(t)$, not used in figures or summaries, was calculated with fluorescence records not normalized. This yielded slightly different results, as normalization by $F_0(x)$ removes the unequal weighting of different regions according to the intensity of their staining.

The silicone-clamp technique

The silicone-clamp technique was used following the methods described by Jacquemond (1997) and initially implemented in our laboratory by S. Pouvreau (University of Bordeaux, Bordeaux, France). Cells, stained as described above, were placed in a stage chamber with the coverslip bottom covered by a thin layer of silicone grease and covered with additional grease, leaving free an end segment of ∼100 µm. The voltage clamp was first established with an Axopatch 200B system (Molecular Devices), using a glass micropipette of 1–3 MΩ, containing "I clamp" solution (largely potassium glutamate), inserted through the grease-covered membrane region at 100–150 µm from the edge of the grease-free region. Then the mode was switched to current clamp and the cell was held nominally at V_m between −80 and −85 mV. In this condition, the grease-free region of the cell was stimulated to produce trains of action potentials by applying trains of current pulses while simultaneously recording current, pipette voltage, and line-scan images. In this configuration, the cells remained stable for >30 min, as reflected in the stability of the small holding current and the reproducibility of the measured action potentials.

Contractile force measurement

The three middle heads of mouse FDB, tied together, were suspended between an ergometer motor (Model 352; Cambridge Technology) and a fixed post. The muscle was adjusted to the optimal length by administering a series of tetanic contractions (supramaximal voltage applied via platinum wire electrodes using 800 ms, 70 Hz train) and selecting the length and resting tension that elicited peak force. The muscle was then stimulated for 3 min with either 40 or 70 Hz trains of 350 ms duration administered every 2 s. Recovery force was measured at 1, 2, 5, and 10 min.

Estimating dye concentration

A proportional measure of dye concentration was obtained with the "invariant" (Launikonis et al., 2005), a linear combination of F_{22} and F_{11} that is proportional to [dye], by a factor that remains unknown. Take for example the fluorescence transients plotted in Fig. 8 C; the sum

$$F_{22}(t) / F_{22}(0) - 0.66\ F_{11}(t) / F_{11}(0)$$

will be insensitive to voltage changes. Multiplying both terms in expression 10 by $F_{22}(0)$, we obtain

$$F_{22}(t) - \left[0.66\ F_{22}(0) / F_{11}(0)\right] F_{11}(t).$$

This is the invariant linear combination, proportional to dye concentration (as it has dimensions of fluorescence) and still insensitive to voltage.

Solutions

Tyrode's (in mM): 140 NaCl, 5 KCl, 2.5 $CaCl_2$, 2 $MgCl_2$, and 10 Hepes. pH was set to 7.2 with NaOH and osmolality to 320 mOsm with NaCl. For force measurements with whole muscles, Tyrode's solution was modified as follows: 137 NaCl, 4 KCl, 2 $CaCl_2$, 1 $MgCl_2$, 1 KH_2PO_4, and 12 $NaHCO_3$, continuously oxygenated. External for voltage clamp experiments: 140 TEA-CH_3SO_3, 1 $CaCl_2$, 3.5 $MgCl_2$, 10 Hepes, 1 4-AP, 0.5 $CdCl_2$, 0.3 $LaCl_3$, 25 µM BTS, and 1 µM TTX (citrate). pH was adjusted to 7.2 with TEA-OH and osmolality to 320 mOsm with TEA methanesulfonate.

Internal (in pipette): 110 *N*-methylglucamine, 110 L-glutamic acid, 10 EGTA, 10 Tris, 10 glucose, 5 Na ATP, 3.55 $CaCl_2$, 7.21 $MgCl_2$, and 10 PC Tris (nominal free [Mg^{2+}] 1 mM and free [Ca^{2+}] 100 nM). pH was set to 7.2 with NaOH and osmolality to 320 mOsm with NMG-glutamate.

Internal for I clamp: 140 potassium glutamate, 2 EGTA, 5 PC-Tris, 0.72 $CaCl_2$, 5.89 $MgCl_2$, 10 PC Tris (nominal free [Mg^{2+}] 1 mM and free [Ca^{2+}] 100 nM), and 5 Na ATP. pH was set to 7.2 with KOH and osmolality to 320 mOsm with potassium glutamate.

This work was supported by grants from the National Institute of Arthritis and Musculoskeletal and Skin Diseases (AR049184 and AR032808 to E. Ríos).

We are grateful to Marino DiFranco and Julio Vergara for providing spectral data on di-8-ANEPPS, to Lee Peachey (University of Pennsylvania) for allowing us to use and modify his classical drawing in Fig. 1 E, to Clara Franzini Armstrong for help in modifying it, to Sandrine Pouvreau (Université Bordeaux 2) for help with the silicone-clamp technique, to Roman Shirokov (University of Medicine and Dentistry, New Jersey) and Bruce Bean (Harvard University) for advice on current clamp methods, and to Lothar Blatter (Rush University) for an insightful critique of the manuscript.

Sharona E. Gordon served as editor.

Submitted: 16 November 2012
Accepted: 25 January 2013

REFERENCES

Allen, D.G., G.D. Lamb, and H. Westerblad. 2008. Skeletal muscle fatigue: cellular mechanisms. *Physiol. Rev.* 88:287–332. http://dx.doi.org/10.1152/physrev.00015.2007

Allen, D.G., E. Clugston, Y. Petersen, I.V. Röder, B. Chapman, and R. Rudolf. 2011. Interactions between intracellular calcium and phosphate in intact mouse muscle during fatigue. *J. Appl. Physiol.* 111:358–366. http://dx.doi.org/10.1152/japplphysiol.01404.2010

Beach, J.M., E.D. McGahren, J. Xia, and B.R. Duling. 1996. Ratiometric measurement of endothelial depolarization in arterioles with a potential-sensitive dye. *Am. J. Physiol.* 270:H2216–H2227.

Bedlack, R.S. Jr., M. Wei, and L.M. Loew. 1992. Localized membrane depolarizations and localized calcium influx during electric field-guided neurite growth. *Neuron.* 9:393–403. http://dx.doi.org/10.1016/0896-6273(92)90178-G

Bradley, J., R. Luo, T.S. Otis, and D.A. DiGregorio. 2009. Submillisecond optical reporting of membrane potential in situ using a neuronal tracer dye. *J. Neurosci.* 29:9197–9209. http://dx.doi.org/10.1523/JNEUROSCI.1240-09.2009

Bullen, A., and P. Saggau. 1999. High-speed, random-access fluorescence microscopy: II. Fast quantitative measurements with voltage-sensitive dyes. *Biophys. J.* 76:2272–2287. http://dx.doi.org/10.1016/S0006-3495(99)77383-2

Chanda, B., R. Blunck, L.C. Faria, F.E. Schweizer, I. Mody, and F. Bezanilla. 2005. A hybrid approach to measuring electrical activity in genetically specified neurons. *Nat. Neurosci.* 8:1619–1626. http://dx.doi.org/10.1038/nn1558

Cohen, L.B., and B.M. Salzberg. 1978. Optical measurement of membrane potential. *Rev. Physiol. Biochem. Pharmacol.* 83:35–88.

Cramér, H. 1946. Tests for significance of parameters, Section 31-3. *In* Mathematical Methods of Statistics. Princeton University Press, Princeton. 465–467.

DiFranco, M., and J.L. Vergara. 2011. The Na conductance in the sarcolemma and the transverse tubular system membranes of mammalian skeletal muscle fibers. *J. Gen. Physiol.* 138:393–419. http://dx.doi.org/10.1085/jgp.201110682

DiFranco, M., J. Capote, and J.L. Vergara. 2005. Optical imaging and functional characterization of the transverse tubular system of mammalian muscle fibers using the potentiometric indicator di-8-ANEPPS. *J. Membr. Biol.* 208:141–153. http://dx.doi.org/10.1007/s00232-005-0825-9

DiFranco, M., A. Herrera, and J.L. Vergara. 2011. Chloride currents from the transverse tubular system in adult mammalian skeletal muscle fibers. *J. Gen. Physiol.* 137:21–41. http://dx.doi.org/10.1085/jgp.201010496

Erlichman, J.S., A.C. Boyer, P. Reagan, R.W. Putnam, N.A. Ritucci, and J.C. Leiter. 2009. Chemosensory responses to CO2 in multiple brain stem nuclei determined using a voltage-sensitive dye in brain slices from rats. *J. Neurophysiol.* 102:1577–1590. http://dx.doi.org/10.1152/jn.00381.2009

Fluhler, E., V.G. Burnham, and L.M. Loew. 1985. Spectra, membrane binding, and potentiometric responses of new charge shift probes. *Biochemistry.* 24:5749–5755. http://dx.doi.org/10.1021/bi00342a010

Fromherz, P., and A. Lambacher. 1991. Spectra of voltage-sensitive fluorescence of styryl-dye in neuron membrane. *Biochim. Biophys. Acta.* 1068:149–156. http://dx.doi.org/10.1016/0005-2736(91)90203-K

Fromherz, P., G. Hübener, B. Kuhn, and M.J. Hinner. 2008. ANNINE-6plus, a voltage-sensitive dye with good solubility, strong membrane binding and high sensitivity. *Eur. Biophys. J.* 37:509–514. http://dx.doi.org/10.1007/s00249-007-0210-y

González, J.E., and R.Y. Tsien. 1995. Voltage sensing by fluorescence resonance energy transfer in single cells. *Biophys. J.* 69:1272–1280. http://dx.doi.org/10.1016/S0006-3495(95)80029-9

González, J.E., and R.Y. Tsien. 1997. Improved indicators of cell membrane potential that use fluorescence resonance energy transfer. *Chem. Biol.* 4:269–277. http://dx.doi.org/10.1016/S1074-5521(97)90070-3

Gross, E., R.S. Bedlack Jr., and L.M. Loew. 1994. Dual-wavelength ratiometric fluorescence measurement of the membrane dipole potential. *Biophys. J.* 67:208–216. http://dx.doi.org/10.1016/S0006-3495(94)80471-0

Gupta, R.K., B.M. Salzberg, A. Grinvald, L.B. Cohen, K. Kamino, S. Lesher, M.B. Boyle, A.S. Waggoner, and C.H. Wang. 1981. Improvements in optical methods for measuring rapid changes in membrane potential. *J. Membr. Biol.* 58:123–137. http://dx.doi.org/10.1007/BF01870975

Heiny, J.A., F.M. Ashcroft, and J. Vergara. 1983. T-system optical signals associated with inward rectification in skeletal muscle. *Nature.* 301:164–166. http://dx.doi.org/10.1038/301164a0

Hübener, G., A. Lambacher, and P. Fromherz. 2003. Anellated hemicyanine dyes with large symmetrical solvatochromism of

absorption and fluorescence. *J. Phys. Chem. B.* 107:7896–7902. http://dx.doi.org/10.1021/jp0345809

Jacquemond, V. 1997. Indo-1 fluorescence signals elicited by membrane depolarization in enzymatically isolated mouse skeletal muscle fibers. *Biophys. J.* 73:920–928. http://dx.doi.org/10.1016/S0006-3495(97)78124-4

Jalife, J. 2000. Ventricular fibrillation: mechanisms of initiation and maintenance. *Annu. Rev. Physiol.* 62:25–50. http://dx.doi.org/10.1146/annurev.physiol.62.1.25

Kao, W.Y., C.E. Davis, Y.I. Kim, and J.M. Beach. 2001. Fluorescence emission spectral shift measurements of membrane potential in single cells. *Biophys. J.* 81:1163–1170. http://dx.doi.org/10.1016/S0006-3495(01)75773-6

Kim, A.M., and J.L. Vergara. 1998. Supercharging accelerates T-tubule membrane potential changes in voltage clamped frog skeletal muscle fibers. *Biophys. J.* 75:2098–2116. http://dx.doi.org/10.1016/S0006-3495(98)77652-0

Knisley, S.B., R.K. Justice, W. Kong, and P.L. Johnson. 2000. Ratiometry of transmembrane voltage-sensitive fluorescent dye emission in hearts. *Am. J. Physiol. Heart Circ. Physiol.* 279:H1421–H1433.

Kuhn, B., P. Fromherz, and W. Denk. 2004. High sensitivity of Stark-shift voltage-sensing dyes by one- or two-photon excitation near the red spectral edge. *Biophys. J.* 87:631–639. http://dx.doi.org/10.1529/biophysj.104.040477

Launikonis, B.S., J. Zhou, L. Royer, T.R. Shannon, G. Brum, and E. Ríos. 2005. Confocal imaging of [Ca2+] in cellular organelles by SEER, shifted excitation and emission ratioing of fluorescence. *J. Physiol.* 567:523–543. http://dx.doi.org/10.1113/jphysiol.2005.087973

Loew, L.M., and L.L. Simpson. 1981. Charge-shift probes of membrane potential: a probable electrochromic mechanism for p-aminostyrylpyridinium probes on a hemispherical lipid bilayer. *Biophys. J.* 34:353–365. http://dx.doi.org/10.1016/S0006-3495(81)84854-0

Montana, V., D.L. Farkas, and L.M. Loew. 1989. Dual-wavelength ratiometric fluorescence measurements of membrane potential. *Biochemistry.* 28:4536–4539. http://dx.doi.org/10.1021/bi00437a003

Morgan, D., M. Capasso, B. Musset, V.V. Cherny, E. Ríos, M.J. Dyer, and T.E. DeCoursey. 2009. Voltage-gated proton channels maintain pH in human neutrophils during phagocytosis. *Proc. Natl. Acad. Sci. USA.* 106:18022–18027. http://dx.doi.org/10.1073/pnas.0905565106

Musset, B., D. Morgan, V.V. Cherny, D.W. MacGlashan Jr., L.L. Thomas, E. Ríos, and T.E. DeCoursey. 2008. A pH-stabilizing role of voltage-gated proton channels in IgE-mediated activation of human basophils. *Proc. Natl. Acad. Sci. USA.* 105:11020–11025. http://dx.doi.org/10.1073/pnas.0800886105

Peachey, L.D. 1965. The sarcoplasmic reticulum and transverse tubules of the frog's sartorius. *J. Cell Biol.* 25:209–231. http://dx.doi.org/10.1083/jcb.25.3.209

Peterka, D.S., H. Takahashi, and R. Yuste. 2011. Imaging voltage in neurons. *Neuron.* 69:9–21. http://dx.doi.org/10.1016/j.neuron.2010.12.010

Pouvreau, S., B. Allard, C. Berthier, and V. Jacquemond. 2004. Control of intracellular calcium in the presence of nitric oxide donors in isolated skeletal muscle fibres from mouse. *J. Physiol.* 560:779–794. http://dx.doi.org/10.1113/jphysiol.2004.072397

Rohr, S., and B.M. Salzberg. 1994. Multiple site optical recording of transmembrane voltage (MSORTV) in patterned growth heart cell cultures: assessing electrical behavior, with microsecond resolution, on a cellular and subcellular scale. *Biophys. J.* 67:1301–1315. http://dx.doi.org/10.1016/S0006-3495(94)80602-2

Royer, L., S. Pouvreau, and E. Ríos. 2008. Evolution and modulation of intracellular calcium release during long-lasting, depleting depolarization in mouse muscle. *J. Physiol.* 586:4609–4629. http://dx.doi.org/10.1113/jphysiol.2008.157990

Siegel, M.S., and E.Y. Isacoff. 1997. A genetically encoded optical probe of membrane voltage. *Neuron.* 19:735–741. http://dx.doi.org/10.1016/S0896-6273(00)80955-1

Sjulson, L., and G. Miesenböck. 2007. Optical recording of action potentials and other discrete physiological events: a perspective from signal detection theory. *Physiology (Bethesda).* 22:47–55. http://dx.doi.org/10.1152/physiol.00036.2006

Tian, Q., M. Oberhofer, S. Ruppenthal, A. Scholz, V. Buschmann, H. Tsutsui, A. Miyawaki, A. Zeug, P. Lipp, and L. Kaestner. 2011. Optical action potential screening on adult ventricular myocytes as an alternative QT-screen. *Cell. Physiol. Biochem.* 27:281–290. http://dx.doi.org/10.1159/000327954

Tsien, R.Y., and J.E. González. 2006. Detection of transmembrane potentials by optical methods. US Patent 7118899, filed December 31, 2002, and issued October 10, 2006.

Valverde, C.A., D. Kornyeyev, M. Ferreiro, A.D. Petrosky, A. Mattiazzi, and A.L. Escobar. 2010. Transient Ca^{2+} depletion of the sarcoplasmic reticulum at the onset of reperfusion. *Cardiovasc. Res.* 85:671–680. http://dx.doi.org/10.1093/cvr/cvp371

Vitha, M.F., and R.J. Clarke. 2007. Comparison of excitation and emission ratiometric fluorescence methods for quantifying the membrane dipole potential. *Biochim. Biophys. Acta.* 1768:107–114. http://dx.doi.org/10.1016/j.bbamem.2006.06.022

Wang, D., Z. Zhang, B. Chanda, and M.B. Jackson. 2010. Improved probes for hybrid voltage sensor imaging. *Biophys. J.* 99:2355–2365. http://dx.doi.org/10.1016/j.bpj.2010.07.037

Zecevic, D., M. Djurisic, L.B. Cohen, S. Antic, M. Wachowiak, C.X. Falk, and M.R. Zochowski. 2003. Imaging nervous system activity with voltage-sensitive dyes. *Curr. Protoc. Neurosci.* Chapter 6: 6: 17.

Zhang, J., R.M. Davidson, M.D. Wei, and L.M. Loew. 1998. Membrane electric properties by combined patch clamp and fluorescence ratio imaging in single neurons. *Biophys. J.* 74:48–53. http://dx.doi.org/10.1016/S0006-3495(98)77765-3